Toxicology 396–397 (2018) 13–22

Contents lists available at ScienceDirect

Toxicology

journal homepage: www.elsevier.com/locate/toxicol

Evaluation of the treatment with resveratrol-loaded nanoparticles in intestinal injury model caused by ischemia and reperfusion

Stephanie Carvalho Borges[a], Paulo Emílio Botura Ferreira[b], Luisa Mota da Silva[c], Maria Fernanda de Paula Werner[d], Juan Manuel Irache[e], Osvaldo Albuquerque Cavalcanti[f], Nilza Cristina Buttow[a,*]

[a] Department of Morphological Sciences, State University of Maringá, Colombo Avenue, 5790, CEP: 87020-900, Maringá, Paraná, Brazil
[b] Campus Uruguaiana, Federal University of Pampa, BR 472 – Km 592, CEP: 97508-000, Uruguaiana, Rio Grande do Sul, Brazil
[c] Postgraduate Program in Pharmaceutical Sciences, University Vale of Itajaí, Uruguai Street, 458, CEP: 88302-901, Itajaí, Santa Catarina, Brazil
[d] Department of Pharmacology, Federal University of Paraná, XV de Novembro Street, 1299, CEP 80.060-000, Curitiba, Paraná, Brazil
[e] Department of Pharmacy and Pharmaceutical Technology, School of Pharmacy, University of Navarra, C/Irunlarrea 1, E-31008, Pamplona, Spain
[f] Department of Pharmacology and Therapeutics, State University of Maringá, Colombo Avenue, 5790, CEP: 87020-900, Maringá, Paraná, Brazil

ARTICLE INFO

Keywords:
Nanoparticles
Poly(anhydride)
Cytotoxicity
Oxidative stress
Resveratrol
Enteric neuron

ABSTRACT

The gastrointestinal tract is extremely sensitive to ischemia and reperfusion (I/R). Studies have reported that resveratrol (RSV) is able to combat damage caused by intestinal I/R. Because of its effectiveness in increasing the permanence and bioavailability of resveratrol in the intestinal epithelium, we investigated whether the effect of resveratrol-loaded in poly(anhydride) nanoparticles reduce oxidative stress and promote myenteric neuroprotection in the ileum of rats subjected to I/R. Physicochemical evaluations were performed on nanoparticles. The animals were divided into nine groups (n = 6/group) and treated every 48 h. Treatments with resveratrol (7 mg/kg of body weight) were applied 5 days before surgery and continued for 7 days after surgery (reperfusion period). The superior mesenteric artery was occluded to cause I/R injury. Oxidative stress, myeloperoxidase, nitrite, aspartate aminotransferase, alanine aminotransferase, immunolabeling of myenteric neurons and glial cells, and gastrointestinal transit was evaluated. Both nanoparticle formulations presented negative charge with homogeneous distribution, and the payload, showed an encapsulation efficiency of 60%. Resveratrol administered in free form prevented alterations that were caused by I/R. The results of the groups treated with RSV-loaded nanoparticles presented similar results to the group treated with free resveratrol. Treatment with empty nanoparticles showed that poly(anhydride) is not an ideal nanocarrier for application in *in vivo* models of intestinal I/R injury, because of hepatotoxicity that may be caused by epithelial barrier dysfunction that triggers the translocation of nanoparticles.

1. Introduction

Ischemia/reperfusion (I/R) is a pathological condition that is initially characterized by the restriction of blood flow, followed by subsequent restoration (Eltzschig and Eckle, 2011). Several clinical events, such as surgery, transplantation, accidents, and visceral atherosclerosis, can result in I/R. The gastrointestinal tract is extremely sensitive to I/R. Injury to the intestines mainly affects the mucosa and enteric nervous system (Borges et al., 2016; Marosti et al., 2015), including enteric glial cells, the expression of vasoactive intestinal polypeptide (VIP), neuronal nitric oxide synthase (nNOS)-immunoreactive nitrergic neurons (Calcina et al., 2005), and the general population of HuC/D-immunoreactive neurons (Borges et al., 2016), which altogether can impair gastrointestinal transit (Calcina et al., 2005; Rivera et al., 2012). In addition to the activation of proinflammatory cytokines (Eltzschig and Eckle, 2011), I/R induces the production of free radicals that can overwhelm the neutralizing capacity of endogenous antioxidants. These free radicals exert their deleterious (Bhattacharyya et al., 2014; Grace, 1994) actions by promoting lipid peroxidation and generating oxidative stress (da Silva de Souza et al., 2015).

Previous studies have reported that oral treatment with 10 mg/kg resveratrol (RSV) in rats combats oxidative stress in animals that are subjected to intestinal I/R (Borges et al., 2016; da Silva de Souza et al., 2015). Resveratrol (3,5,4′-trihydroxy-*trans*-stilbene) is a polyphenol that is found mainly in grape seeds and red wine and has antioxidant and antiinflammatory activity (Kumar and Sharma, 2010). Kumar and

* Corresponding author.
E-mail address: ncbuttow@uem.com (N.C. Buttow).

https://doi.org/10.1016/j.tox.2018.02.002
Received 11 December 2017; Received in revised form 31 January 2018; Accepted 5 February 2018
Available online 07 February 2018
0300-483X/

Sharma (2010) suggested that RSV eliminates free radicals and increases the levels of antioxidant enzymes by neutralizing oxidative stress and promoting neuroprotection. One of the main difficulties of using RSV orally is its short half-life, in which it is rapidly metabolized (Walle et al., 2004). In order to solve this drawback, the use of nanoparticles with bioadhesive properties have been proposed (Penalva et al., 2015). In fact, these nanocarriers may be useful to significantly prolong the residence time of the dosage form in close contact with the absorptive epithelium and, in addition, control the release of the cargo. As a consequence, these nanoparticulate drug delivery systems may be of interest to improve the efficacy of resveratrol as potential treatment for gastrointestinal sections affected by I/R.

In this context, the main objective of this work was to evaluate the capability of resveratrol nanoencapsulated in poly(anhydride) nanoparticles as treatment to reduce the oxidative stress and to afford myenteric neuroprotection in the ileum of rats subjected to I/R. For this purpose, nanoparticles based on the combination between Gantrez® AN [poly(anhydride)] and hydroxypropyl-β-cyclodextrin (HPβCD) were selected as delivery systems for resveratrol. On one hand, poly(anhydride) nanoparticles based on Gantrez® AN display high bioadhesive properties (Agüeros et al., 2011). On the other hand, the use of the oligosaccharide is based on its ability to promote the payload of low absorption compounds in polymer nanoparticles (Agüeros et al., 2011) as well as on its capability to inhibit the effect of intestinal P-glycoprotein and cytochrome P450 enzymatic complexes (Agüeros et al., 2010, 2011), that have the ability to metabolize and promote the extrusion of drugs and other compounds from the epithelium to the intestinal lumen (Agüeros et al., 2010, 2011).

2. Materials and methods

2.1. Preparation of RSV-loaded nanoparticles (RSV-NP)

Resveratrol (Galena. Campinas, SP, Brazil; lot no. C20110928) and HPβCD (Sigma-Aldrich. Steinheim, Germany), (0.3:1 molar proportion) were dispersed in 2 mL of ethanol for 15 min and then in 5 mL of acetone that contained 100 mg of previously dissolved poly(anhydride) (Poly(methyl vinyl ether-co-maleic anhydride) (poly[anhydride]; Gantrez® AN 119; molar weight, 200,000) ISP (Koln, Germany)). The mixture was magnetically stirred for 15 min at room temperature. Nanoparticles were formed by the addition of 20 mL of a mixture with ethanol:ultrapure water (1:1, v/v). The organic solvents were evaporated under vacuum at 45 °C in a rotary evaporator (Büchi R-144, Switzerland). The resulting nanoparticles were purified by both slow and rapid centrifugation (3,000 × *g* for 4 min and 21,000 × *g* for 20 min). The supernatants were removed and the pellets resuspended in water. The formulations were frozen and lyophilized (Genesis 12EL, Virtis, USA) using 5% sucrose (p/p) as the cryoprotectant. As control, empty nanoparticles (NP) were prepared in the same way as described above but in the absence of RSV.

2.1.1. Physicochemical characterization

The mean hydrodynamic diameter of the nanoparticles and their zeta potential were determined by photon correlation spectroscopy and electrophoretic laser Doppler anemometry, respectively, using a Zetaplus analyzer (Brookhaven Instruments, USA). The diameter of the nanoparticles was determined after dispersion in ultrapure water (1:10) and measured at 25 °C by dynamic light scattering angle of 90 °C. The polydispersity index (PDI), which indicates the homogeneity of this distribution, was also calculated. The zeta potential was determined as follows: 200 µL of the samples were diluted in 2 mL of a 0.1 mM KCL solution. The yield of the process was calculated by gravimetry as described previously by Arbós and colleagues (Arbós et al., 2003). The formulations were measured in triplicate, and the results are expressed as mean ± standard error.

2.1.2. Morphological analysis

The morphology of the nanoparticles was analyzed and photographed using a scanning electron microscope (Zeiss DMS 940A SEM; Oberkochen, Germany) with a digital image capture system (Point Electronic GmBh, Halle, Germany). Lyophilized nanoparticles were resuspended in ultrapure water and centrifuged at 27,000 × *g* for 20 min at 4 °C. The supernatants were then discarded, and pellets were assembled on a glass plate and adhered with double-sided adhesive tape on dry metal bases under warm airflow. Finally, the nanoparticles were covered with a thin 12 nm layer of gold using an Emitech K550 cathode pulverizer device (Emitech, UK). The micrographs were obtained under the following conditions: 10 kV and 5000X of 9 mm distance.

2.1.3. Resveratrol quantification

Samples of lyophilized nanoparticles were centrifuged, and the pellets were solubilized in acetonitrile (3/4, v/v) for nanoparticle rupture. The amount of encapsulated RSV was determined by an ultraviolet-visible spectrum spectrophotometer at 305 nm using a calibration curve performed under a range of 0.6–7 µg/mL ($r^2 > 0.997$) in acetonitrile (3/4, p/v). The results are expressed as µg of RSV/mg of nanoparticles. The encapsulation efficiency (EE) was calculated using the following equation: EE (%) = (Encapsulated RSV weight/Initial RSV weight) × 100.

2.2. Animals and experimental protocol

We used 54 male albino Wistar rats (*Rattus norvegicus*; 255 ± 2.704 g). The animals were obtained from the Central Bioterium of the Universidade Estadual de Maringá and housed in the Sectorial Room of the Department of Morphological Sciences. During the treatment period, they remained in an environment at 22 °C ± 2 °C with a 12 h/12 h light/dark cycle. The animal procedures were approved by the Committee of Ethics in the Use of Animals of the University State of Maringá (opinion no. 149/2013) and were in accordance with the ethical principles adopted by the Brazilian Society of Science in Laboratory Animals (SBCAL/COBEA).

The animals received standard rodent chow (NUVILAB, recommended by the National Research Council and U.S. National Institutes of Health) and water *ad libitum*. The animals were divided into nine groups ($n = 6$/group) and treated every 48 h. Treatment began 5 days before surgery and continued for 7 days after surgery (reperfusion period). The animals were treated by gavage with 7 mg/kg resveratrol (in free or nanoencapsulated form; Table 1). Free resveratrol was diluted in 10% grain alcohol and 90% water. The nanoparticles were diluted only in water. The C, SC, and IRC groups were treated with a solution that contained only vehicle: 10% grain alcohol and 90% water before and after surgery.

2.3. Induction of ischemia

Prior to surgery, all of the animals were fasted for 15 h. After the

Table 1
Experimental groups and treatments. S: sham; IR: ischemia/reperfusion.

Groups		SMA[a]	Treatment
C	Not operated	–	Vehicle
SC	Underwent surgery	Not occluded	Vehicle
STR	Underwent surgery	Not occluded	Free resveratrol (unencapsulated)
STEN	Underwent surgery	Not occluded	Empty nanoparticle
STRN	Underwent surgery	Not occluded	Resveratrol – loaded nanoparticle
IRC	Underwent surgery	Occluded	Vehicle
IRTR	Underwent surgery	Occluded	Free resveratrol (unencapsulated)
IRTEN	Underwent surgery	Occluded	Empty nanoparticle
IRTRN	Underwent surgery	Occluded	Resveratrol – loaded nanoparticle

[a] SMA superior mesenteric artery.

animals were intramuscularly anesthetized with a mixture of 20 mg/kg xylazine (Sespo Industry and Commerce, Paulínia, SP, Brazil) and 100 mg/kg ketamine (Sespo Industry and Commerce, Paulínia, SP, Brazil), all of the groups except for the control group underwent abdominal laparotomy.

We occluded the superior mesenteric artery using a microvascular clamp to cause I/R injury, and lateral irrigation between the ischemic and non-ischemic regions was blocked by loops. After 45 min of ischemia, the clamp and loops were removed, and blood flow was re-established. The abdomen was sutured with 3-0 nylon thread. During the 7-day reperfusion period, the animals remained in individual cages.

2.4. Gastrointestinal transit analysis

For the analysis of gastrointestinal transit, 300 μL of a solution that contained 3% Carmin hydro and 0.5% ethylcellulose (Corantec, São Paulo, Brazil) diluted in water was administered orally 48 h before euthanasia. The animals were placed in individual cages with free access to food and water. For this analysis, the latency (in min) for the animal to eliminate the first fecal pellet that contained the colorant was recorded.

2.5. Blood and ileum sampling

After being anesthetized with a lethal dose of 120 mg/kg thiopental sodium (Cristália Pharmaceutical and Chemicals Products, Brazil), 5 mL of blood was collected from each animal and centrifuged for 10 min at 3000 × *g*. The resulting plasma was used to determine the levels of aspartate aminotransferase (AST) and alanine aminotransferase (ALT) using commercial Analisa® kits with the aid of a spectrophotometer (Bioplus2000, São Paulo, Brazil) at a wavelength of 340 nm. The distal portion of the ileum was collected, fractionated, and processed for evaluate the biochemical markers of oxidative stress and inflammatory parameters and for immunofluorescence staining of myenteric neuronal and glial population.

2.6. Biochemical assays

2.6.1. Reduced glutathione and lipid hydroperoxide levels

The ileum was weighed and homogenized in 200 mM potassium phosphate buffer (pH 6.5). The reaction of GSH with 5,5′-dithiobis-2-nitrobenzoic acid was read at 412 nm. Individual values were interpolated based on a GSH standard curve and are expressed as μg of GSH/g of tissue.

The other part of the homogenate was centrifuged for 20 min at 9000 × *g*, and part of the supernatant was used to determine lipid hydroperoxide (LOOH) levels according to Jiang et al. (Jiang et al., 1991). Readings were performed at 560 nm using a spectrophotometer. LOOH concentrations were determined using an extinction coefficient of 4.3 mmolar 1/cm, and the results are expressed as mmol/mg of tissue.

2.6.2. Superoxide dismutase and glutathione s-transferase enzymatic activity

After the ileum was homogenized in 200 mM potassium phosphate buffer (pH 6.5) and centrifuged, the resulting supernatant was collected to perform the biochemical assays to determine the enzymatic activity of superoxide dismutase (SOD) and glutathione s-transferase (GST). The enzymatic assay for SOD is based on the ability of SOD to inhibit the autooxidation of pyrogallol (Marklund and Marklund, 1974). Readings were performed at 405 nm using a spectrophotometer. The results are expressed as U of SOD/mg of protein. The enzymatic activity of GST was determined according to the method of Warholm et al. (Warholm et al., 1985). Readings were performed at 340 nm using a spectrophotometer, with an extinction coefficient of 9.6 mmolar 1/cm. The results are expressed as μmol/min/mg of protein.

2.6.3. Myeloperoxidase enzyme activity

The precipitate from ileum homogenate centrifugation was resuspended in 80 mM potassium phosphate buffer that contained 0.5% hexadecyltrimethylammonium. The samples were homogenized and centrifuged for 20 min at 11,000 × *g* at 4 °C. The reaction was performed in a 96-well plate using tetramethylbenzidine. Enzymatic activity of myeloperoxidase (MPO) was determined at 620 nm using a spectrophotometer. The results are expressed as units of optical density (OD)/min/mg of protein.

2.6.4. Determination of nitrite levels

Nitric oxide levels were measured based on the total nitrite estimation that was obtained by the Greiss reaction, adapted from the method of Tiwari et al. (Tiwari et al., 2011). A portion of the ileum was homogenized in 0.1 M sodium phosphate buffer solution (PBS) pH 7.4 and centrifuged for 10 min at 3000 × *g*. Subsequently, 50 μL of this supernatant was added to 50 μL of Greiss reagent (i.e., a solution that contained phosphoric acid, sulfanilamide, and *N*-1-naphthalylethylenediamide) and measured in 96-well plates at 570 nm using a spectrophotometer. Nitrite concentrations were calculated using a standard curve that was located in the range of 100 to 1.56 μM of sodium nitrite ($NaNO_2$). Nitrite levels are expressed as μM.

2.7. Immunohistochemistry

After washing in 0.1 M PBS (pH 7.4) and fixed for 3 h in 4% paraformaldehyde solution (pH 7.4), the intestine was cut into transverse segments and dissected using tweezers under a stereomicroscope.

2.7.1. Evaluation of huC/D- and nNOS-immunoreactive myenteric neurons, VIPergic varicosities, and S100- and GFAP-immunoreactive glial cells

Whole-mounts of the muscular tunica from the distal ileum of each animal underwent immunohistochemistry to label the general population of myenteric neurons (HuC/D-immunoreactive), subpopulation of nitrergic neurons (nNOS-immunoreactive), vasoactive intestinal polypeptide (VIP)-ergic varicosities, and enteric glial cells (S100- and glial fibrillary acid protein [GFAP]-immunoreactive) in the muscular tunica. Double-labeling of HuC/D + nNOS and GFAP + S100 and single-labeling of VIPergic varicosities were performed.

The segments were washed twice for 10 min in 0.1 M PBS (pH 7.4) and Triton-X100 with 0.5% PBS-T and then incubated for 1 h in blocking solution that contained 2% bovine serum albumin (BSA) and 10% donkey serum in PBS-T. Double-labeling was performed using the following primary antibodies: anti-HuC/D (1:600, mouse, catalog no. A21271, Molecular Probes, Invitrogen, Eugene, OR, USA), anti-nNOS (1:500, goat, catalog no. SC-49055, Santa Cruz Biotechnology, Santa Cruz, CA, USA), anti-glial fibrillary acidic protein (GFAP; 1:700, goat, ab53554, Abcam), anti-S100 (1:400, rabbit, catalog no. 18-0046, Molecular Probes, Invitrogen, Eugene, OR, USA), and anti-VIP (1:400, rabbit, catalog no. T-4245, Peninsula Laboratories). Incubation with the primary antibodies was maintained for 48 h at room temperature under stirring. The incubation substrate consisted of PBS-T, 2% BSA, and 2% donkey serum.

After incubation with the primary antibody, the membranes were washed three times in PBS-T for 10 min. They were then incubated with the following secondary antibodies for 2 h in the dark: anti-mouse (1:500, Alexa Fluor 488, Molecular Probes, Invitrogen, Eugene, OR, USA), anti-goat (1:500, Alexa Fluor 568, Molecular Probes, Invitrogen, Eugene, OR, USA), and anti-rabbit (1:500, Alexa Fluor 488, Molecular Probes, Invitrogen, Eugene, OR, USA). The incubation substrate consisted of PBS-T, 2% BSA, and 2% donkey serum. The membranes were then washed three times in PBS-T for 10 min and attached on histological slides that contained Antifade® (Life Technologies of Brazil Comm. Ind. Prod. Biotec. Ltda, SP, Brazil), stored under refrigeration, and protected from light.

2.7.2. Quantitative analysis of myenteric neurons and glial cells

Quantitative analyses were performed using samples of the total membrane preparations, based on images that were captured using a high-resolution camera coupled to an FSX100 fluorescence microscope (Olympus). The images were later analyzed using ImagePro Plus 4.5.029 software (Media Cybernetics, Silver Spring, MD, USA). For HuC/D, nNOS, and S100 quantification, all of the neurons or glial cells that were evident in 30 images that were captured with a 20× objective were counted. The area of each image was approximately 0.14725 mm^2, and the total area quantified was 4.41768 mm^2. The results are expressed as neurons/cm^2.

2.7.3. Morphometric analysis of immunoreactive neurons and myenteric varicosities

To assess the morphometry of the neuronal populations of the myenteric plexus, images that were captured with a 20× objective were analyzed using ImagePro Plus software. For HuC/D- and nNOS-immunoreactive neurons, the area of 100 cell bodies per animal was measured. The area of 400 VIPergic varicosities per animal were also measured using images that were captured with a 40× objective. The morphometric results are expressed as μm^2.

2.7.4. Fluorescence analysis of glial fibrillary acidic protein

GFAP immunolabeling was performed using membrane preparations to assess the intensity of fluorescence. Thirty ganglia per animal were captured using a 20× objective. The images were captured using the same high-resolution camera and fluorescence microscope that was described above for the quantitative analyses. The exposure time, brightness, contrast, and focus adjustment were maintained for all of the photomicrographs. ImageJ 1.43 software (National Institutes of Health, Bethesda, MD, USA) was used to measure the intensity of GFAP immunolabeling based on red-green-blue (RGB).

2.8. Statistical analysis

The statistical analysis was performed using GraphPad Prism 5 software. The results are expressed as mean ± standard error. For comparisons between groups with a normal distribution of data, one-way analysis of variance (ANOVA) was performed, followed by Tukey's *post hoc* test. The Kruskal-Wallis nonparametric test was applied to data that had a non-normal distribution, followed by Dunn's *post hoc* test. Values of $p < 0.05$ were considered statistically significant.

3. Results

3.1. Physicochemical characterization of nanoparticles

The physicochemical characteristics of the nanoparticle formulations employed in this work are presented in Table 2. The loading of resveratrol on poly(anhydride) nanoparticles importantly increased the mean size of the resulting nanocarriers (234 nm for RSV-NP vs 169 for NP) but has negligible effects on the zeta potential and polydispersity of the resulting nanocarriers. Thus, both nanoparticle formulations displayed a negative charge with a homogeneous distribution (PDI below 0.2). Regarding the payload, the amount of nanoencapsulated RSV was calculated to be close to 60 µg per mg nanoparticle with an encapsulation efficiency of 60%.

The size of the nanoparticles that were observed by scanning electron microscopy (SEM) was similar to that observed by photon correlation spectroscopy, presenting a spherical shape. The RSV-NP displayed a rough surface.

3.2. Levels of AST and ALT

The levels of AST and ALT in the IRTEN (Table 1) group were significantly higher than in the other groups ($p < 0.001$; Fig. 1). In the other groups, no significant alterations were observed compared with the C group ($p > 0.05$; Fig. 1).

3.3. Biochemical tests

Fig. 2a shows the increase in SOD activity in the IRC group compared with the C and STR groups ($p < 0.05$). The IRTR and IRTRN groups presented results that were similar to the C group and significantly different from the IRC group ($p < 0.05$). The other groups did not present significant differences from the C group ($p > 0.05$; Fig. 2a). No significant differences in GST and MPO enzymes were observed between groups ($p > 0.05$; Fig. 2c, e).

Among the sham groups, GSH levels were significantly lower in the STEN group than in the C and STR groups ($p < 0.01$) and significantly lower in the STRN group than in the C group ($p < 0.01$) and STR group ($p < 0.05$). Among the I/R groups, a decrease in GSH levels was observed in the IRC group compared with the C and STR groups ($p < 0.01$). A decrease in GSH levels was observed in the IRTEN group compared with the C group ($p < 0.001$), STR group ($p < 0.001$), and SC group ($p < 0.05$). A decrease in GSH levels was observed in the IRTRN group compared with the C and STR groups ($p < 0.05$). The IRTR group presented results that were similar to the C group but significantly different from the STEN and STRN groups ($p < 0.05$). Among the I/R groups, GSH levels in the IRTR group differed significantly from the IRC group ($p < 0.05$) and IRTEN group ($p < 0.01$). The IRTRN group presented no significant difference in GSH levels compared with the IRC, IRTEN, or IRTR group ($p > 0.05$; Fig. 2b).

An increase in LOOH levels was observed in the STEN group ($p < 0.05$) and IRC group ($p < 0.01$) compared with the C group. The IRC group also presented an increase in LOOH levels compared with the SC group ($p < 0.05$). The other groups did not present significant differences in LOOH levels compared with the C or SC group ($p > 0.05$). The IRTR, IRTEN, and IRTRN groups also did not present significant differences in LOOH levels compared with the IRC group ($p > 0.05$; Fig. 2d).

Nitrite levels in the IRTEN group were significantly higher than in the C group ($p < 0.001$), STR group ($p < 0.001$), STRN group ($p < 0.001$), and IRC group ($p < 0.05$; Fig. 2f). The IRTR and IRTRN groups presented results that were similar to the C group ($p > 0.05$) but significantly different from the IRTEN group ($p < 0.001$). The other groups presented no significant differences in nitrite levels ($p > 0.05$; Fig. 2f).

3.4. Immunohistochemistry

3.4.1. Quantitative and morphometric analysis of myenteric neurons

According to the density of the general neuronal population (HuC/D-immunoreactive) analysis among the sham groups, only the STEN

Table 2
Physico-chemical characterization of nanoparticles. NP: empty nanoparticles; RSV-NP: resveratrol-loaded nanoparticles. Data expressed as mean ± standard error, n = 3.

	Diameter (nm)	PDI[a]	Zeta potential (mV)	Gravimetric yield (%)	RSV complexed (µg/mg NP)	Encapsulation efficiency (E.E%)
NP	169 ± 2.2	0.13	−45.2 ± 0.44	90.5 ± 2.3	–	–
RSV-NP	234 ± 1.5	0.17	−50 ± 0.72	76 ± 1.1	60 ± 2.9	60 ± 2.95

[a] PDI Polydispersity index.

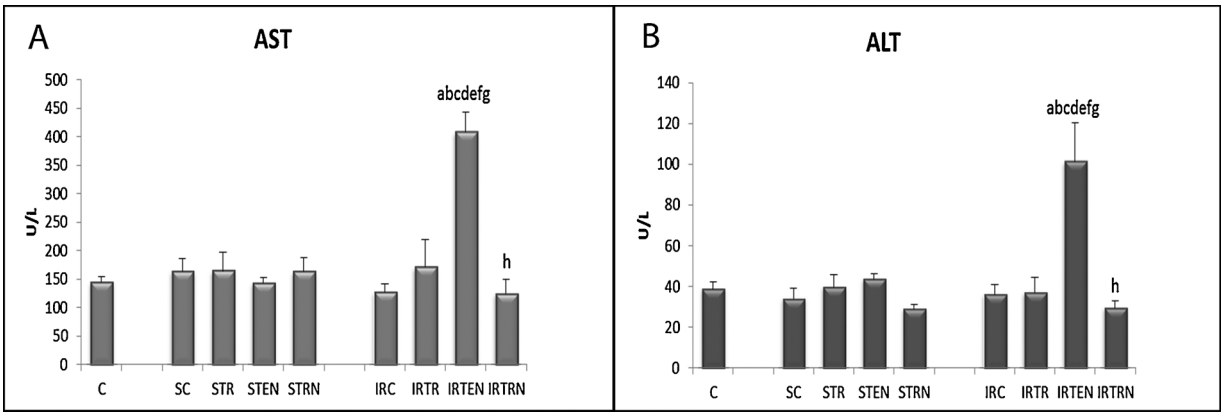

Fig. 1. Levels of aspartate aminotransferase (AST) and alanine aminotransferase (ALT). [a]Significant difference from C group. [b]Significant difference from SC group. [c]Significant difference from STR group. [d]Significant difference from STEN group. [e]Significant difference from STNR group. [f]Significant difference from IRC group. [g]Significant difference from IRTR group. [h]Significant difference group IRTEN group. The data are expressed as mean ± standard error ($n = 6$).

group presented a lower density compared with the C group ($p < 0.01$) and SC group ($p < 0.05$). Among the I/R groups, a lower overall neuronal density was observed in the IRC and IRTRN groups compared with the C group ($p < 0.05$), and a lower density was observed in the IRTEN group compared with the C group ($p < 0.01$), SC group ($p < 0.05$), STR group ($p < 0.05$), and STRN group ($p < 0.05$). The IRTR group presented results that were similar to the C group ($p > 0.05$). The IRTR group had a higher neuronal density than the IRC group ($p < 0.05$) and IRTEN group ($p < 0.01$). The IRTRN group did not present a significant difference from the IRC, IRTEN, or IRTR group ($p > 0.05$; Fig. 3d).

Among the sham and I/R groups, the density of the nitrergic subpopulation (nNOS-immunoreactive) was not significantly different between groups ($p > 0.05$; Fig. 3e). Double-labeling revealed that the proportion of nitrergic neuron densities relative to the general neuronal population was approximately 16% in the C, SC, STR, STRN, and IRTR groups. An increase in this proportion (approximately 20%) was observed in the groups that exhibited neuronal loss (STEN, IRC, IRTEN, and IRTRN groups).

No change in the general population of HuC/D-immunoreactive neurons was observed in the sham groups (SC, STR, STEN, and STRN groups; $p > 0.05$). Among the I/R groups, only the IRTEN group presented an increase in the neuronal profile compared with the C group ($p < 0.05$), STR group ($p < 0.001$), and STRN group ($p < 0.01$; Fig. 3f).

The nitrergic subpopulation (nNOS-immunoreactive) presented an increase in neuronal profile in the SC group ($p < 0.05$) and STR group ($p < 0.001$) compared with the C group. All of the I/R groups presented an increase in the neuronal profile of the nitrergic subpopulation compared with the C and SC groups ($p < 0.001$). Compared with the STR group, a significant difference was found in the IRC group ($p < 0.001$), IRTEN group ($p < 0.001$), IRTR group ($p < 0.01$), and IRTRN group ($p < 0.01$). The I/R groups also presented an increase in the nitrergic neuronal profile compared with the STEN and STRN groups ($p < 0.001$). No significant difference in the nitrergic neuronal profile was observed among the I/R groups ($p > 0.05$; Fig. 3g).

Among the sham groups, the area of VIPergic varicosities increased in the STR group compared with the SC group ($p < 0.01$) and increased in the STEN group compared with the C and SC groups ($p < 0.001$). The STRN group presented a VIPergic varicosity profile that was similar to the C and SC groups but a significantly smaller area compared with the STEN group ($p < 0.01$). All of the I/R groups presented an increase in VIPergic varicosities compared with the C and SC group ($p < 0.001$). The IRC group ($p < 0.05$), IRTEN group ($p < 0.05$), and IRTR group ($p < 0.01$) presented a significant increase in VIPergic varicosities compared with the STR group. Compared with the STRN group, the IRC group ($p < 0.001$), IRTR group ($p < 0.001$), IRTRN group ($p < 0.001$), and IRTEN group ($p < 0.05$) presented an increase in VIPergic varicosities. No significant differences in VIPergic varicosities were found among the I/R groups ($p > 0.05$; Fig. 4b).

3.4.2. Quantitative analysis and fluorescence intensity of myenteric glial cells

The assessment of myenteric glial cells (S100-immunoreactive) revealed an increase in density in the STEN group ($p < 0.01$), IRTRN group ($p < 0.01$), IRC group ($p < 0.001$), and IRTEN group ($p < 0.001$) compared with the C and SC groups. The IRC and IRTEN groups ($p < 0.01$) also exhibited glial cell proliferation compared with the STR group. The STEN group ($p < 0.05$), IRTRN group ($p < 0.05$), IRC group ($p < 0.001$), and IRTEN group ($p < 0.001$) also presented a significant increase in glial cell density compared with the STRN group. The IRTR group maintained glial cell density that was similar to the C, IRC, and IRTRN groups but significantly lower than the IRTEN group ($p < 0.05$; Fig. 5d).

The analysis of the mean fluorescence intensity of GFAP immunoreactivity among the sham groups revealed an increase in the STEN group compared with the C and STR groups ($p < 0.001$). The STR group presented a lower fluorescence intensity compared with the SC group ($p < 0.001$). The STRN group presented a lower fluorescence intensity compared with the SC group ($p < 0.01$) and STEN group ($p < 0.001$). Among the I/R groups, the IRC group presented an increase in fluorescence intensity compared with the C, STR, and STRN groups ($p < 0.001$), and the IRTEN group presented an increase in fluorescence intensity compared with the SC group ($p < 0.01$), C group ($p < 0.001$), STR group ($p < 0.001$), and STRN group ($p < 0.001$). The IRTR and IRTRN groups presented a mean fluorescence intensity that was similar to the C group but different from the STEN group ($p < 0.001$). Among the I/R groups, the IRTR and IRTRN groups presented a lower fluorescence intensity compared with the IRC and IRTEN groups ($p < 0.001$; Fig. 5e).

3.5. Gastrointestinal transit analysis

The IRC and IRTEN groups presented a longer gastrointestinal transit time compared with the C and SC groups ($p < 0.001$). The IRC group presented a longer gastrointestinal transit time compared with the STR group ($p < 0.01$) and STRN group ($p < 0.05$). The IRTEN group presented a longer gastrointestinal transit time compared with the STR group ($p < 0.001$) and STRN group ($p < 0.01$). Among the I/R groups, the IRTR and IRTRN groups presented gastrointestinal transit times that were similar to the C group (Fig. 6).

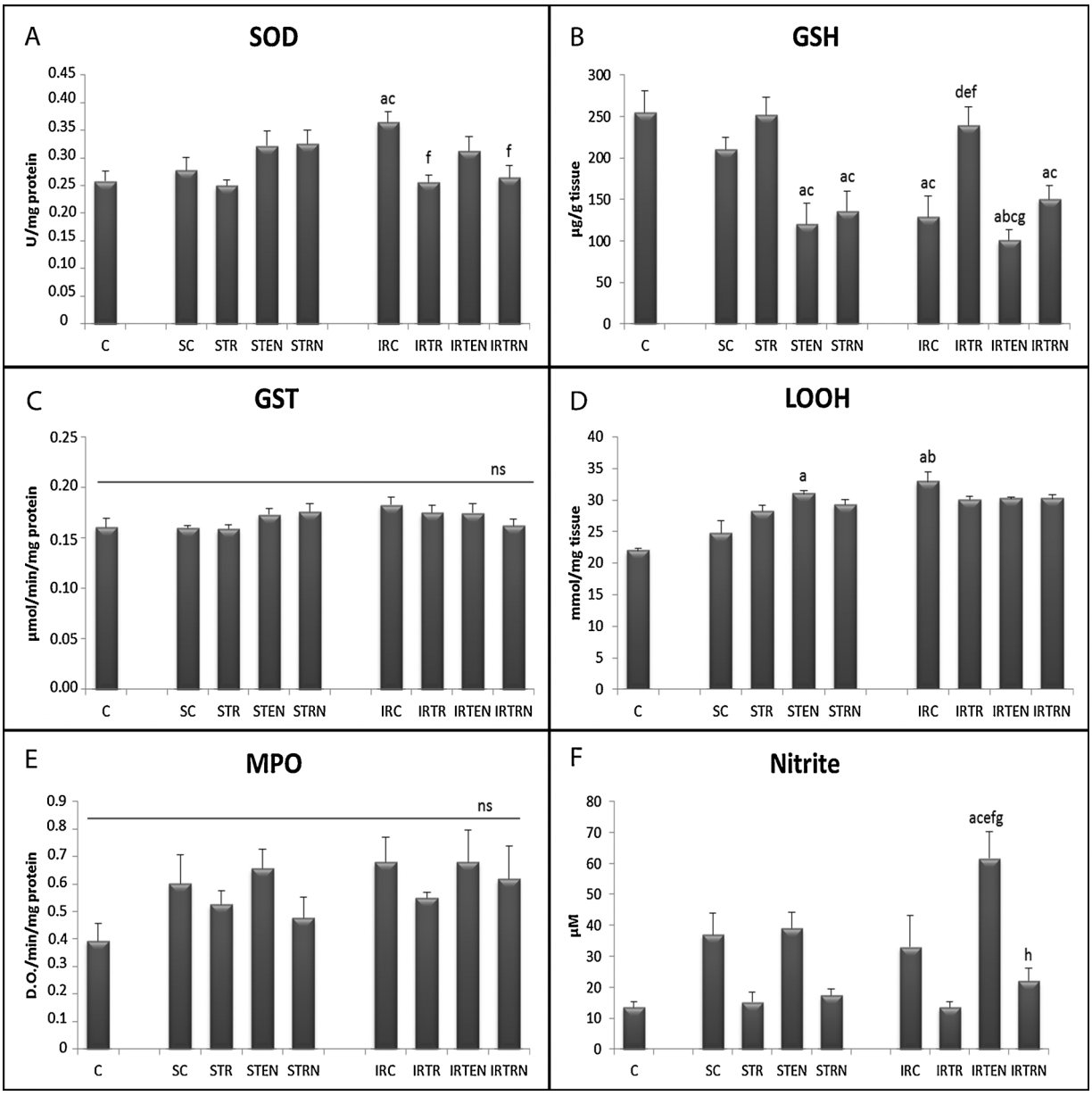

Fig. 2. Biochemical assays. Enzymatic activity of superoxide dismutase (SOD) (a), glutathione *S*-transferase (GST) (c), and myeloperoxidase (MPO) (e). Levels of non-protein sulfhydryl groups (GSH) (b), lipid hydroperoxides (LOOH) (d), and nitrite (f). [a]Significant difference from C group. [b]Significant difference from SC group. [c]Significant difference from STR group. [d]Significant difference from STEN group. [e]Significant difference from STNR group. [f]Significant difference from IRC group. [g]Significant difference from IRTR group. [h]Significant difference from IRTEN group. [ns]Not significant. The data are expressed as mean ± standard error ($n = 6$).

4. Discussion

The present study found that 45 min of ischemia followed by 7 days of reperfusion promoted oxidative stress, loss of the general population of myenteric neurons, an increase in the neuronal profile of the nitrergic subpopulation and VIPergic varicosities, glial cell proliferation (S100-immunoreactive), reactive gliosis (GFAP-immunoreactive), and a longer gastrointestinal transit time. Several pathophysiological processes are involved in I/R injury. Ischemia is associated with significant alterations in the transcriptional control of gene expression (i.e., transcriptional reprogramming), which can lead to the activation of programmed cell death (Eltzschig and Eckle, 2011). The reperfusion period after ischemia is characterized by a substantial increase in free radicals that promote further tissue injury. In the present study, these pathophysiological alterations led to a significant decrease (to 23%) of the general population of myenteric neurons (HuC/D-immunoreactive) compared with the control group. Other studies also reported myenteric neuron death after 7 days of reperfusion (Borges et al., 2016; Marosti et al., 2015). In the present study, the analysis of the density of the nitrergic subpopulation revealed no significant differences between groups. Therefore, neuronal loss likely occurred because of the continuous formation of reactive species and progression to a condition of oxidative stress, which has been previously observed in studies of I/R-related injury (Bhattacharyya et al., 2014; da Silva de Souza et al., 2015).

The present study found high levels of oxidative stress in the intestinal wall in the IRC group. The enzymatic activity of SOD in the IRC group was 41% higher than in the control group. Some authors have reported a decrease in SOD activity during periods of ischemia followed by reperfusion up to 12 h (Brahmbhatt et al., 2013; Liu et al., 2015). After 7 days of reperfusion, modulation of the antioxidant system may favor the increase in SOD activity to eliminate superoxide radicals that are still produced. Similarly, the tripeptide GSH is used as an indicator of oxidative stress, acting as an electron donor to eliminate peroxides

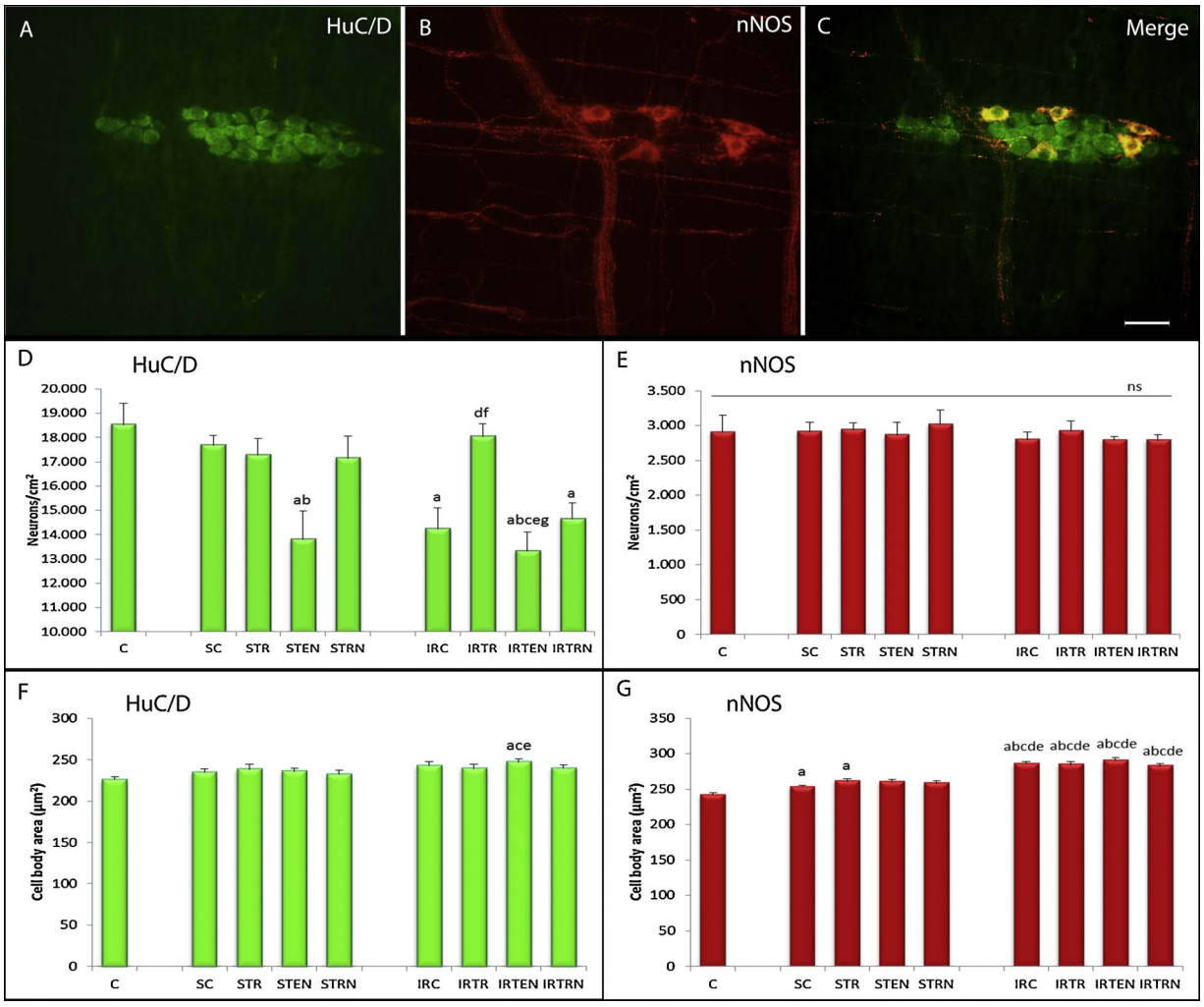

Fig. 3. Photomicrographs showing fluorescence of myenteric neurons that were immunoreactive to HuC/D (a) and nNOS (b) proteins and double-labeled with HuC/D and nNOS (c). Calibration bar = 50 µm. (d, e) Density of the general neuronal population (d) and nitrergic subpopulation (e). (f, g) Mean area of neuronal cell bodies of the general neuronal population (f) and nitrergic subpopulation (g). [a]Significant difference from C group. [b]Significant difference from SC group. [c]Significant difference from STR group. [d]Significant difference from STEN group. [e]Significant difference from STNR group. [f]Significant difference from IRC group. [g]Significant difference from IRTR group. [ns]Not significant. The data are expressed as mean ± standard error (n = 6).

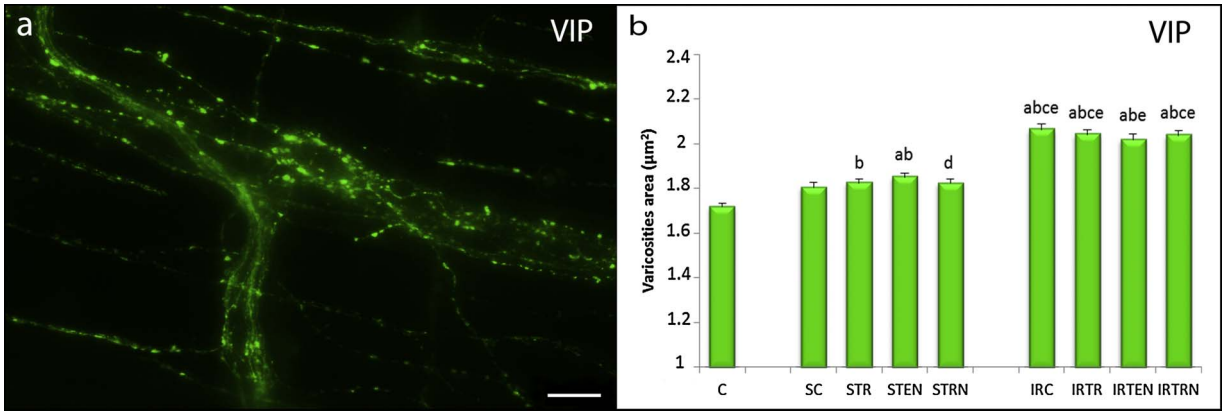

Fig. 4. Photomicrograph showing fluorescence of myenteric VIPergic varicosities (a). Calibration bar = 20 µm. Mean area of myenteric VIPergic varicosities (b). [a]Significant difference from C group. [b]Significant difference from SC group. [c]Significant difference from STR group. [d]Significant difference from STEN group. [e]Significant difference from STNR group. The data are expressed as mean ± standard error (n = 6).

and other reactive species. Reduced glutathione levels in the IRC group decreased approximately 50% compared with the control group. Low levels of GSH in the gut in rats that are subjected to I/R have been previously reported (da Silva de Souza et al., 2015; Karabulut et al., 2006). Lipid peroxidation is one of the outcomes of the actions of reactive species, and LOOH levels are an indirect measure of damage that is caused by oxidative stress (Orsu et al., 2013). IRC group displayed a 49% increase in LOOH levels, compared with the control group. The

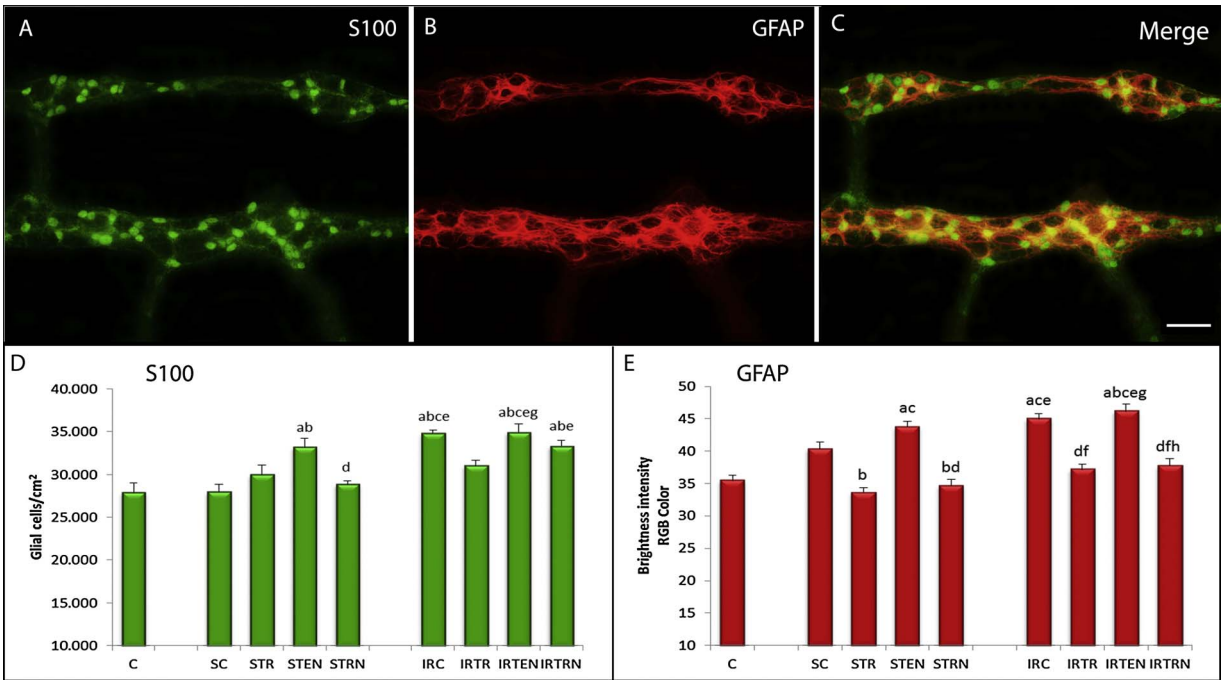

Fig. 5. Photomicrographs showing fluorescence of myenteric glial cells immunoreactive to S100 (a) and GFAP (b) proteins and double-labeling of S100 and GFAP (c). Calibration bar = 50 μm. (d) Density of myenteric glial cells (d). (e) Fluorescence intensity of GFAP protein. [a]Significant difference from C group. [b]Significant difference from SC group. [c]Significant difference from STR group. [d]Significant difference from STEN group. [e]Significant difference from STNR group. [f]Significant difference from IRC group. [g]Significant difference from IRTR group. [h]Significant difference from IRTEN group. The data are expressed as mean ± standard error (n = 6).

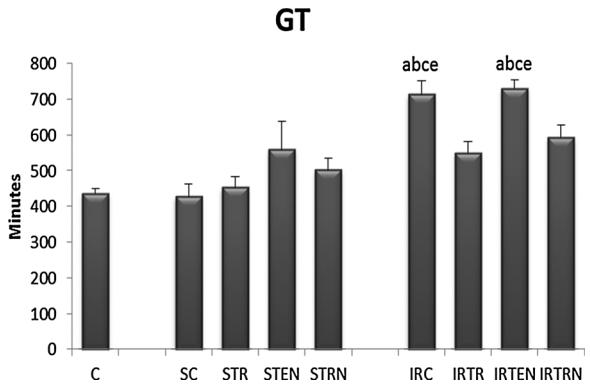

Fig. 6. Gastrointestinal transit. [a]Significant difference from C group. [b]Significant difference from SC group. [c]Significant difference from STR group. [d]Significant difference from STEN group. [e]Significant difference from STNR group. The data are expressed as mean ± standard error (n = 6).

antioxidant enzyme GST is responsible for detoxifying xenobiotic compounds and lipid hydroperoxides. We found high levels of lipid peroxidation in the IRC group but no significant changes in GST activity. Oxidative stress can occur through inflammatory reactions, among other factors, after injury. Several authors have reported that injury that is caused by ischemia followed by reperfusion up to 24 h increased MPO activity (Lin et al., 2014; Yildiz et al., 2009). After 7 days of reperfusion, we found that the activity of this inflammatory enzyme did not significantly change, but other inflammatory parameters that were not assessed in the present study may be related to I/R-induced injury.

Among the alterations that are caused by I/R injury, the present study found an 18% increase in the nitrergic neuronal profile in the IRC group compared with the control group. These alterations likely occurred through oxidative stress or an increase in intracellular Ca^{2+} levels during I/R (Dong et al., 2006; Hossmann, 2006). Excess Ca^{2+} can activate destructive processes, such as enzyme and cytoskeletal protein degradation (Dong et al., 2006). The profile of VIPergic varicosities also presented a 20% increase in the IRC group compared with the control group. Enteric neurons have the ability to increase VIP expression under conditions of stress (Borges et al., 2016; Sand et al., 2008), and the increase in VIPergic varicosities may represent a defense mechanism of the enteric nervous system in response to I/R (Borges et al., 2016). Vasoactive intestinal polypeptide also stimulates astrocyte proliferation in the central nervous system (Delgado and Ganea, 2003). In the present study, we observed an increase in the profile of VIPergic varicosities in the enteric nervous system and further found that I/R injury significantly increased glial cell proliferation (S100 immunoreactivity) by 24% and increased the fluorescence intensity of GFAP immunoreactivity (reactive gliosis) by 26%. Alterations in the enteric glial cell population may be related to neuroinflammation and neurodegenerative processes (Bradley et al., 1997) that are promoted by I/R.

Previous studies reported delays in gastrointestinal transit that occur as a consequence of cellular and tissue alterations that are promoted by I/R (Calcina et al., 2005; Rivera et al., 2012). We observed significant slowing of gastrointestinal transit in the IRC group compared with the control group. Several factors may contribute to the increase in gastrointestinal transit time, including oxidative stress, inflammation (Lubbers et al., 2010), and glial (McClain et al., 2014) and enteric neuron dysfunction (Calcina et al., 2005).

The pathophysiological changes that are caused by I/R may be potentially ameliorated by resveratrol (Borges et al., 2016; da Silva de Souza et al., 2015). In order to improve the efficacy of resveratrol, one possible strategy may be its encapsulation into polymeric nanoparticles with bioadhesive properties. In this context, in the present work, the ability of poly(anhydride) nanoparticles combined with HPβCD has been evaluated.

The group that was subjected to I/R and treated with RSV-NP (IRTRN group) presented SOD activity, LOOH levels, nitrite levels, an HuC/D-immunoreactive cell profile, GFAP fluorescence intensity, and gastrointestinal transit time that were similar to the control group. However, this treatment was unable to prevent all the damage that was

caused by I/R. The I/R group that was treated with RSV-NP (IRTRN group) presented an approximately 20% loss of myenteric neurons compared with the control group. We also observed increases in the nitrergic neuronal profile, VIPergic varicosities, and glial cell proliferation (S100 immunoreactivity) and a decrease in GSH activity. This partial protection by RSV-NP may be explained by the findings in the I/R group that was treated with empty nanoparticles (IRTEN group). The IRTEN group presented a significant 182% increase in AST levels (i.e., a nonspecific marker of hepatic injury) and 160% increase in ALT levels (i.e., a specific marker of hepatic parenchymal injury) compared with the control group. Animals that were subjected to I/R and treated with NP presented hepatotoxicity. In the I/R group that was treated with RSV-NP (IRTRN group), AST and ALT levels were similar to the control group. The IRTRN group may have been protected by the antiinflammatory and antioxidant actions of resveratrol itself. These results appeared to contradict previous results by Ojer and collaborators (Ojer et al., 2012) who described poly(anhydride) nanoparticles containing HPβCD (NP in the present work) as safe when orally administered in rats (Ojer et al., 2012). This apparent discrepancy would be related with the fact that the present I/R model promotes the destruction of intestinal cells and negatively affect to the mucosal integrity, leading to an increase in intestinal epithelial permeability and dysfunction (Eltzschig and Eckle, 2011; Lin et al., 2014). Therefore, this disruption of intestinal epithelium would facilitate the passage of nanoparticles and their arrival to the liver, inducing hepatotoxicity (e.g., increased levels of AST and ALT). This idea would be supported by the fact that it has been described that in I/R model animals, the translocation of bacteria and endotoxins is facilitated (Lin et al., 2014; Tassopoulos et al., 2016).

In addition to causing liver damage, we also found that the empty nanoparticles promoted intestinal injury. The I/R group that was treated with empty nanoparticles (IRTEN group) presented 28% loss of the general neuronal population compared with the control group. It also presented increases in the general neuronal profile, nitrergic subpopulation, VIPergic varicosities, glial cell proliferation (S100-immunoreactive), and reactive gliosis (GFAP-immunoreactive), a decrease in GSH levels, and a delay in gastrointestinal transit. The IRTEN group also exhibited a substantial 352% increase in nitrite levels. We assessed nitrite levels as a secondary indicator of the presence of nitric oxide (NO) in intestinal tissue. Excess NO can cause cellular and tissue damage (Kobayashi, 2010; Kubes and McCafferty, 2000) and result in formation of the peroxynitrite radical ($ONOO^-$), a powerful oxidizing agent (Rivera et al., 2011). Excess nitrite in the IRTEN group may have been an inflammatory response to I/R, followed by the translocation of empty nanoparticles and consequently toxicity in tissue.

The empty nanoparticles also promoted damage in the sham group. The STEN group presented overall neuronal loss of 25% compared with the control group. We also observed increases in the profile of VIPergic varicosities, glial cell proliferation (S100-immunoreactive), and reactive gliosis (GFAP-immunoreactive). The sham group that was treated with empty nanoparticles also exhibited oxidative stress in ileal tissue. The sham group that was treated with empty nanoparticles presented a significant 40% increase in lipid peroxidation (LOOH levels) and 52% decrease in GSH activity compared with the control group. These alterations in the sham group were attenuated by treatment with RSV-NP. With the exception of GSH levels, the sham group that was treated with RSV nanoparticles (STRN group) presented a general neuronal density, VIPergic varicosity profile, glial cell density (S100-immunoreactive), GFAP fluorescence intensity (GFAP-immunoreactive), and LOOH levels that were similar to the control group.

Resveratrol treatment in the STRN and IRTRN groups appeared to be responsible for attenuation of the adverse effects of I/R. The alterations that were caused by I/R were attenuated or even prevented by RSV in free form. In addition to neutralizing free radicals, RSV can activate the synthesis of antioxidant enzymes (Frémont, 2000; Kumar and Sharma, 2010), inhibiting the formation of oxidative stress. The I/R group that was treated with resveratrol in free form (IRTR group) presented SOD activity, GSH activity, LOOH levels, and nitrite levels that were similar to the control group, indicating its antioxidant effects. Treatment with RSV in free form also prevented myenteric neuronal loss, glial cell proliferation, reactive gliosis, and the delay in gastrointestinal transit in the I/R group. Other authors that used the same experimental design and treated I/R animals with 10 mg/kg resveratrol in free form also found that this polyphenol inhibited oxidative stress and promoted neuroprotection (Borges et al., 2016; da Silva de Souza et al., 2015).

Despite the limited intrinsic bioavailability of RSV, the treatment performed with the free form when compared to the nanoencapsulated form, exceeded the capacity to relieve oxidative damage promoted by IR, myenteric and glial neuronal protection, and the maintenance of gastrointestinal transit time. These results, in addition to those of the empty nanoparticles, suggest that poly(anhydride), when applied as a nanoparticulate polymer carrier, fallout into limited results in terms of neuroprotection and reduction of oxidative stress. In the I/R group that was treated with empty nanoparticles (IRTEN group), the poly(anhydride) nanoparticles appeared to translocate, causing high hepatotoxicity and myenteric neuronal loss in animals that were treated with this formulation. Treatment with poly(anhydride) nanoparticles that contained the RSV yielded results that were similar to free resveratrol with regard to neuroprotective and antioxidant effects. Overall, these results indicate that this nanocarrier system is not ideal for the treatment of intestinal injury that is caused by I/R because of hepatotoxicity that may be caused by epithelial barrier dysfunction that triggers the translocation of nanoparticles. Other kinds of nanocarriers may represent possible alternatives to ameliorate RSV administration for intestinal I/R injury.

Ethical conduct of research

All animal studies were performed after approval from the Institutional and Animal Care and Use Committee.

Financial & competing interests disclosure

This work was supported by Coordination of Improvement of Higher Education Personnel (CAPES). Program CAPES-DGU 184/2009.

The authors have no other relevant affiliations or financial involvement with any organization or entity with a financial interest in or financial conflict with the subject matter or materials discussed in the manuscript apart from those disclosed.

Acknowledgements

We thank the Post-Graduation Program in Biological Sciences: Cellular and Molecular Biology of State University of Maringá and Coordination of Improvement of Higher Education Personnel(CAPES). We thank the technicians Maria Eurides Cancino, Maria dos Anjos Fortunato, and Maria Ângela Moreira in the histology laboratory at the State University of Maringá. We also thank Michael Arends for the English review.

References

Agüeros, M., Zabaleta, V., Espuelas, S., Campanero, M.A., Irache, J.M., 2010. Increased oral bioavailability of paclitaxel by its encapsulation through complex formation with cyclodextrins in poly(anhydride) nanoparticles. J. Control. Release 145, 2–8.

Agüeros, M., Espuelas, S., Esparza, I., Calleja, P., Peñuelas, I., Ponchel, G., Irache, J.M., 2011. Cyclodextrin-poly(anhydride) nanoparticles as new vehicles for oral drug delivery. Expert. Opin. Drug. Deliv. 8, 721–734.

Arbós, P., Campanero, M.A., Arangoa, M.A., Renedo, M.J., Irache, J.M., 2003. Influence of the surface characteristics of PVM/MA nanoparticles on their bioadhesive properties. J. Control. Release 89, 19–30.

Bhattacharyya, A., Chattopadhyay, R., Mitra, S., Crowe, S.E., 2014. Oxidative stress: an essential factor in the pathogenesis of gastrointestinal mucosal diseases. Physiol. Rev.

94, 329–354.
Borges, S.C., da Silva de Souza, A.C., Beraldi, E.J., Schneider, L.C., Buttow, N.C., 2016. Resveratrol promotes myenteric neuroprotection in the ileum of rats after ischemia-reperfusion injury. Life. Sci. 166, 54–59.
Bradley, J.S., Parr, E.J., Sharkey, K.A., 1997. Effects of inflammation on cell proliferation in the myenteric plexus of the guinea-pig ileum. Cell. Tissue. Res. 289, 455–461.
Brahmbhatt, V., Oliveira, M., Briand, M., Perrisseau, G., Bastic Schmid, V., Destaillats, F., Pace-Asciak, C., Benyacoub, J., Bosco, N., 2013. Protective effects of dietary EPA and DHA on ischemia-reperfusion-induced intestinal stress. J. Nutr. Biochem. 24, 104–111.
Calcina, F., Barocelli, E., Bertoni, S., Furukawa, O., Kaunitz, J., Impicciatore, M., Sternini, C., 2005. Effect of N-methyl-d-aspartate receptor blockade on neuronal plasticity and gastrointestinal transit delay induced by ischemia/reperfusion in rats. Neuroscience 134, 39–49.
Delgado, M., Ganea, D., 2003. Vasoactive intestinal peptide prevents activated microglia-induced neurodegeneration under inflammatory conditions: potential therapeutic role in brain trauma. FASEB J. 17, 1922–1924.
Dong, Z., Saikumar, P., Weinberg, J.M., Venkatachalam, M.A., 2006. Calcium in cell injury and death. Annu. Rev. Pathol. 1, 405–434.
Eltzschig, H.K., Eckle, T., 2011. Ischemia and reperfusion–from mechanism to translation. Nat. Med. 17, 1391–1401.
Frémont, L., 2000. Biological effects of resveratrol. Life. Sci. 66, 663–673.
Grace, P.A., 1994. Ischaemia-reperfusion injury. Br. J. Surg. 81, 637–647.
Hossmann, K.A., 2006. Pathophysiology and therapy of experimental stroke. Cell. Mol. Neurobiol. 26, 1057–1083.
Jiang, Z.Y., Woollard, A.C., Wolff, S.P., 1991. Lipid hydroperoxide measurement by oxidation of Fe2+ in the presence of xylenol orange: comparison with the TBA assay and an iodometric method. Lipids 26, 853–856.
Karabulut, A.B., Kirimlioglu, V., Kirimlioglu, H., Yilmaz, S., Isik, B., Isikgil, O., 2006. Protective effects of resveratrol on spleen and ileum in rats subjected to ischemia-reperfusion. Transplant. Proc. 38, 375–377.
Kobayashi, Y., 2010. The regulatory role of nitric oxide in proinflammatory cytokine expression during the induction and resolution of inflammation. J. Leukoc. Biol. 88, 1157–1162.
Kubes, P., McCafferty, D.M., 2000. Nitric oxide and intestinal inflammation. Am. J. Med. 109, 150–158.
Kumar, A., Sharma, S.S., 2010. NF-kappaB inhibitory action of resveratrol: a probable mechanism of neuroprotection in experimental diabetic neuropathy. Biochem. Biophys. Res. Commun. 394, 360–365.
Lin, Z.L., Yu, W.K., Tan, S.J., Duan, K.P., Dong, Y., Bai, X.W., Xu, L., Li, N., 2014. Protective effects of terminal ileostomy against bacterial translocation in a rat model of intestinal ischemia/reperfusion injury. World J. Gastroenterol. 20, 17905–17913.
Liu, F.C., Tsai, H.I., Yu, H.P., 2015. Organ-Protective effects of red wine extract, resveratrol, in oxidative stress-Mediated reperfusion injury. Oxid. Med. Cell. Longev. 2015, 568–634.
Lubbers, T., Buurman, W., Luyer, M., 2010. Controlling postoperative ileus by vagal activation. World. J. Gastroenterol. 16, 1683–1687.
Marklund, S., Marklund, G., 1974. Involvement of the superoxide anion radical in the autoxidation of pyrogallol and a convenient assay for superoxide dismutase. Eur. J. Biochem. 47, 469–474.
Marosti, A.R., da Silva, M.V., Palombit, K., Mendes, C.E., Tavares-de-Lima, W., Castelucci, P., 2015. Differential effects of intestinal ischemia and reperfusion in rat enteric neurons and glial cells expressing P2 × 2 receptors. Histol. Histopathol. 30, 489–501.
McClain, J.L., Grubišić, V., Fried, D., Gomez-Suarez, R.A., Leinninger, G.M., Sévigny, J., Parpura, V., Gulbransen, B.D., 2014. Ca2+ responses in enteric glia are mediated by connexin-43 hemichannels and modulate colonic transit in mice. Gastroenterology 146, 497–507 (e491).
Ojer, P., de Cerain, A.L., Areses, P., Peñuelas, I., Irache, J.M., 2012. Toxicity studies of poly(anhydride) nanoparticles as carriers for oral drug delivery. Pharm. Res. 29, 2615–2627.
Orsu, P., Murthy, B.V., Akula, A., 2013. Cerebroprotective potential of resveratrol through anti-oxidant and anti-inflammatory mechanisms in rats. J. Neural. Transm. (Vienna) 120, 1217–1223.
Penalva, R., Esparza, I., Larraneta, E., González-Navarro, C.J., Gamazo, C., Irache, J.M., 2015. Zein-Based nanoparticles improve the oral bioavailability of resveratrol and its anti-inflammatory effects in a mouse model of endotoxic shock. J. Agric. Food Chem. 63, 5603–5611.
Rivera, L.R., Thacker, M., Pontell, L., Cho, H.J., Furness, J.B., 2011. Deleterious effects of intestinal ischemia/reperfusion injury in the mouse enteric nervous system are associated with protein nitrosylation. Cell. Tissue. Res. 344, 111–123.
Rivera, L.R., Pontell, L., Cho, H.J., Castelucci, P., Thacker, M., Poole, D.P., Frugier, T., Furness, J.B., 2012. Knock out of neuronal nitric oxide synthase exacerbates intestinal ischemia/reperfusion injury in mice. Cell. Tissue. Res. 349, 565–576.
Sand, E., Themner-Persson, A., Ekblad, E., 2008. Infiltration of mast cells in rat colon is a consequence of ischemia/reperfusion. Dig. Dis. Sci. 53, 3158–3169.
Tassopoulos, A., Chalkias, A., Papalois, A., Iacovidou, N., Xanthos, T., 2016. The effect of antioxidant supplementation on bacterial translocation after intestinal ischemia and reperfusion. Redox. Rep. 22 (1), 1–9.
Tiwari, V., Kuhad, A., Chopra, K., 2011. Emblica officinalis corrects functional, biochemical and molecular deficits in experimental diabetic neuropathy by targeting the oxido-nitrosative stress mediated inflammatory cascade. Phytother. Res. 25, 1527–1536.
Walle, T., Hsieh, F., DeLegge, M.H., Oatis, J.E., Walle, U.K., 2004. High absorption but very low bioavailability of oral resveratrol in humans. Drug. Metab. Dispos. 32, 1377–1382.
Warholm, M., Guthenberg, C., von Bahr, C., Mannervik, B., 1985. Glutathione transferases from human liver. Methods Enzymol. 113, 499–504.
Yildiz, F., Terzi, A., Coban, S., Celik, H., Aksoy, N., Bitiren, M., Cakir, H., Ozdogan, M.K., 2009. Protective effects of resveratrol on small intestines against intestinal ischemia-reperfusion injury in rats. J. Gastroenterol. Hepatol. 24, 1781–1785.
da Silva de Souza, A.C., Borges, S.C., Beraldi, E.J., de Sá-Nakanishi, A.B., Comar, J.F., Bracht, A., Natali, M.R., Buttow, N.C., 2015. Resveratrol reduces morphologic changes in the myenteric plexus and oxidative stress in the ileum in rats with ischemia/reperfusion injury. Dig. Dis. Sci. 60, 3252–3263.